Directional pumping of water and oil microdroplets on slippery surface

Jieke Jiang[a,1], Jun Gao[b,1], Hengdi Zhang[a], Wenqing He[a], Jianqiang Zhang[a], Dan Daniel[c], and Xi Yao[a,d,2]

[a]Department of Biomedical Sciences, City University of Hong Kong, Kowloon, Hong Kong SAR, People's Republic of China; [b]Physics of Complex Fluids, University of Twente, 7500 Enschede, The Netherlands; [c]Institute of Materials Research and Engineering, 138634 Singapore; and [d]Shenzhen Research Institute, City University of Hong Kong, Shenzhen 518057, People's Republic of China

Edited by David A. Weitz, Harvard University, Cambridge, MA, and approved December 24, 2018 (received for review October 5, 2018)

Transporting water and oil microdroplets is important for applications ranging from water harvesting to biomedical analysis but remains a great challenge. This is due to the amplified contact angle hysteresis and insufficient driving force in the micrometer scale, especially for low-surface energy oil droplets. Coalescence of neighboring droplets, which releases vast additional surface energy, was often required, but its relatively uncontrollable nature brings uncertainties to the droplet motion, and the methodology is not applicable to single droplets. Here we introduce a strategy based on slippery surface with immobilized lubricant menisci to directionally transport microdroplets. By simply mounting hydrogel dots on slippery surface, the raised menisci remotely pump microdroplets via capillary force with high efficiency, regardless of droplet size or surface energy. By proof-of-concept experiments, we demonstrate that our method allows for highly efficient water droplet collection and highly sensitive biomedical analyte detection.

droplet transport | microdroplet | capillary force | slippery surface | antifouling

Directional transport of water and oil droplets without external energy input is crucial in a variety of applications (1), such as microfluidics (2, 3), heat exchangers (4), biomedical analysis (5, 6), and water harvesting (7). The most successful strategies to transport droplets are often inspired by the remarkable liquid collection capabilities of insects and plants, which exploit either a surface energy gradient or an asymmetric geometry to generate a driving force (8–13). However, these strategies generally fail in transporting droplets with diameters of several hundred micrometers or less. This is because at such a small scale, contact angle hysteresis becomes increasingly important, whereas the external driving forces become negligible (14). This challenge is particularly difficult to address for oil droplets transport because most solid surfaces are oleophilic, which dramatically increases the hysteresis.

To address this challenge, there are two optional approaches: either to enhance the driving force or to reduce the contact angle hysteresis. Coalescence of neighboring droplets can be used to generate this enhanced driving force because the reduction in surface area releases additional energy for work, but its wide adoption is precluded by its largely uncontrollable nature and its inapplicability for single droplets (7, 15–18). Alternatively, employing surfaces with low-contact angle hysteresis is a promising approach. Recently, directional driving of oil droplets was demonstrated on a textured oleophobic surface (12), but this strategy requires complicated substrate design and fabrication. A simpler approach is to introduce a liquid layer on a solid material, which results in a defect-free fluid interface with extreme slipperiness to both water and oil, the so-called slippery liquid-infused surface (19). For example, a recent study successfully demonstrated the directional transport of small water droplets on slippery surface with asymmetric bumps (20). However, continuous growth of droplets via condensation or coalescence was still needed to derive sufficient driving force and driving oil droplets remains challenging.

Nature has a smart way to transport small objects on liquid surface. For example, seeds of aquatic plants can be collected by surface-piercing vegetation via capillary force (21, 22), a crucial process in seed dispersal (Fig. 1*A*). Some water-walking insects, particularly the larva of waterlily leaf beetle, prove to be excellent examples of using directional capillary force to transport themselves on the curved menisci from water to dry land (23). The capillary driving strategy is effective for objects with sizes ranging from nanometer to millimeter (24). Herein, inspired by nature, we demonstrate the directional capillary pumping of microdroplets on slippery surfaces, without the need of coalescence or continuous growth (Fig. 1*B*). The maximum pumping distance is determined by capillary length, which is independent to the size and surface tension of droplet, and feature size of mounted hydrogel dots. This enables an unprecedentedly easy and robust strategy to transport different-sized water and oil droplets with minimum substrate preparation.

Results

The slippery surface was made of polydimethylsiloxane (PDMS) infused with silicone oil. Surface-piercing hydrogel dots were inkjet-printed onto the PDMS using a liquid patterning method (25) before infusing with oil (Fig. 1*C*). After oil infusion (oil thickness is typically 20 μm), the hydrogel dots were surrounded by oil menisci, which served as immobilized spots to capture microdroplets (Fig. 1*D* and *SI Appendix*, Fig. S1). After fabrication, the substrate was tilted, and Fig. 1 *E* and *F* show that

Significance

Driving liquid microdroplets has been challenging due to the large contact angle hysteresis and insufficient driving force at microscale. We designed a strategy to directionally transport water and oil microdroplets. By simply mounting hydrogel dots on a slippery surface to arrest lubricant menisci, spontaneously formed capillary force pumps liquid microdroplets continuously at high efficiency. Such strategy is universally applicable to water and oil droplets of different surface tensions and different sizes, yet with little substrate preparation effort. Furthermore, we demonstrated its applications in highly efficient water droplet collection and biomedical sample enrichment for highly sensitive detection. Our technique may be useful in water harvesting, droplet condensation, and biomedical analysis.

Author contributions: X.Y. designed research; J.J., J.G., H.Z., W.H., and J.Z. performed research; J.J., J.G., D.D., and X.Y. analyzed data; J.G. and D.D. set up models and carried out calculation; and J.J., J.G., D.D., and X.Y. wrote the paper.

The authors declare no conflict of interest.

This article is a PNAS Direct Submission.

[1]J.J. and J.G. contributed equally to this work.

[2]To whom correspondence should be addressed. Email: xi.yao@cityu.edu.hk.

This article contains supporting information online at www.pnas.org/lookup/suppl/doi:10.1073/pnas.1817172116/-/DCSupplemental.

Published online January 28, 2019.

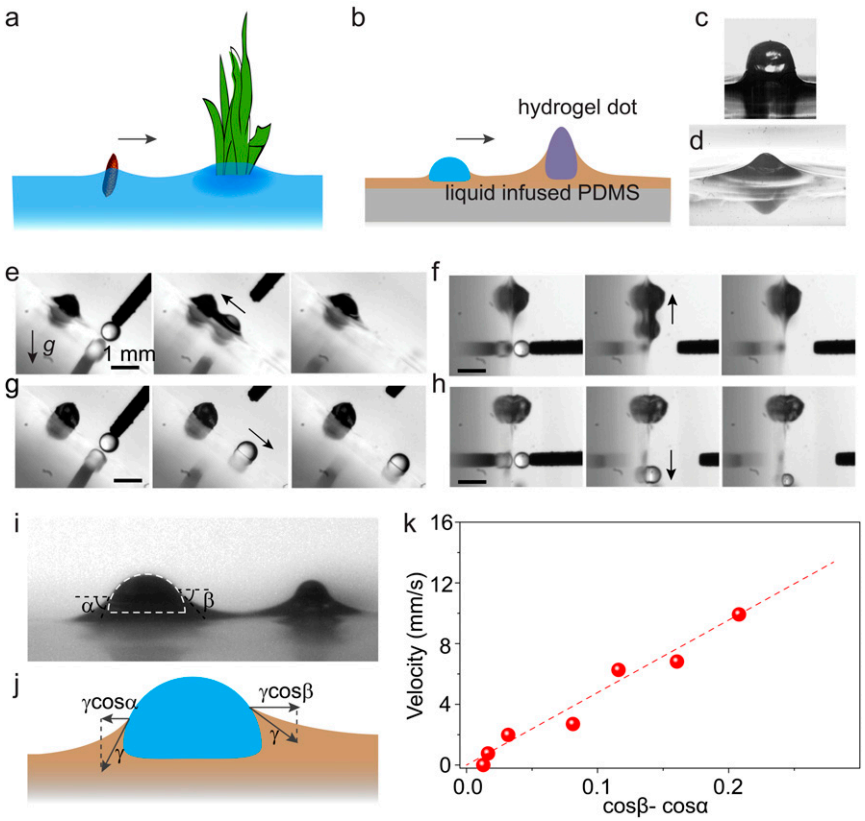

Fig. 1. Directionally pumping droplets by capillary force on slippery surface with immobilized meniscus. (*A*) Schematic shows surface-piercing vegetation capturing floating seeds by capillary force. (*B*) Inspired by this, capillary pumping of microdroplets on slippery surface with immobilized meniscus is developed, whereby a meniscus-immobilizing hydrogel dot captures nearby droplets by capillary force. (*C*) A hydrogel dot was printed on PDMS surface. (*D*) After infusing the surface with silicone oil, the hydrogel dot raises and immobilizes oil meniscus. (*E* and *F*) Mediated by the meniscus, a water microdroplet can be pumped to the hydrogel dot against gravity, whether the slippery surface is tilted by 45° (*E*) or 90° (*F*). (*G* and *H*) In contrast, microdroplets cannot be driven without the oil meniscus. (*I*) Optical images showing a microdroplet (on the left) being driven toward the hydrogel dot (on the right), bridged by the oil meniscus. (*J*) The driving force is due to the net surface tension force projected on the horizontal direction ($\gamma\cos\beta - \gamma\cos\alpha$) exerted on the opposite sides of the droplet. (*K*) cos β–cos α and the velocity of the droplet follow a nearly linear relationship.

water droplets within ∼1 mm distance are driven toward the hydrogel dots against gravity, confirming the effectiveness of our droplet transport strategy. It is noteworthy that the hydrogel dots can be replaced by a glass slide, a glass bead, or any other surface-piercing structures that raise the lubricant meniscus with similar results (*SI Appendix*, Fig. S2). To verify that the driving force is capillarity, we removed the oil meniscus by wiping the lubricant off the surface. Because the capillary force is bridged by the meniscus, this should suppress the capillary force, and indeed, the droplets can no longer be pumped upward (compare Fig. 1 *E* and *G* and Fig. 1 *F* and *H*).

A simplified model can help to rationalize the driving force and the resultant motion, as sketched in Fig. 1*I* (Movie S1) and Fig. 1*J*. We define α and β as the slope angles of the oil menisci to the left and right side of the droplet, respectively. Due to the overlapping and thus elevated oil menisci between the droplet and the hydrogel dot, there is a difference between α and β (α > β), generating an attractive capillary force $F_c > 0$, which drives the microdroplet to the hydrogel dot: $F_c = \gamma R(cos\beta - cos\alpha) > 0$, where γ is the oil/air interfacial tension and R is the droplet size (26–28). At the initial stage when the moving velocity U is low, F_c is balanced by the viscous drag force $F_d \sim \eta RU$, where η = 10 mPa·s is the oil viscosity. Therefore, $U \sim \gamma/\eta$ (cos β − cos α), where $\gamma/\eta \sim 2$ m/s is the characteristic viscocapillary velocity. This model is in agreement with our measured values of (cos β − cos α) and U of a 0.3-mm-diameter droplet during the driving process (Fig. 1*K*). The slope (dashed line in Fig. 1*K*) is 0.05 m/s, which suggests a prefactor of about 0.03 in our model, whereas the classical Stokes flow predicts a prefactor of $1/4\pi \sim 0.08$ (29). This slight disagreement is expected because classical Stokes flow does not account for the wall effect due to the PDMS substrate and the finite gap between the droplet and the hydrogen dot. We also note that in our system the size of the meniscus is comparable to that of the droplet, which was not the case in previous analyses on the viscous dissipation of droplets on slippery surfaces (30, 31).

The maximum droplet driving distance D_{max} is determined by the meniscus length, which we found experimentally to be given by its capillary length $\lambda = (\gamma/\rho g)^{1/2} = 1.5$ mm (Fig. 2*A*), where ρ is the oil density and g is the acceleration due to gravity (32). F_c (and hence also cos β − cos α) is a function of the distance between hydrogel and droplet L. Previous work establishes that F_c decays exponentially for large $L >> \lambda$ and increases dramatically with decreasing L when $L \sim \lambda$ (27, 28), consistent with our experimental observations (*SI Appendix*, Fig. S3).

It is important to note that λ is only dependent on the properties of the infused oil (ρ, γ). This suggests a unique advantage of capillary pumping strategy: it is highly robust and is insensitive to the structure of substrate material and the geometrical, physical, or chemical properties of droplets, even when a wrapping oil layer is formed on the droplet surface when the spreading coefficient is positive.

To test this, we first observed the driving process of 100 droplets with diameters ranging from 0.2 to 1.2 mm deposited with

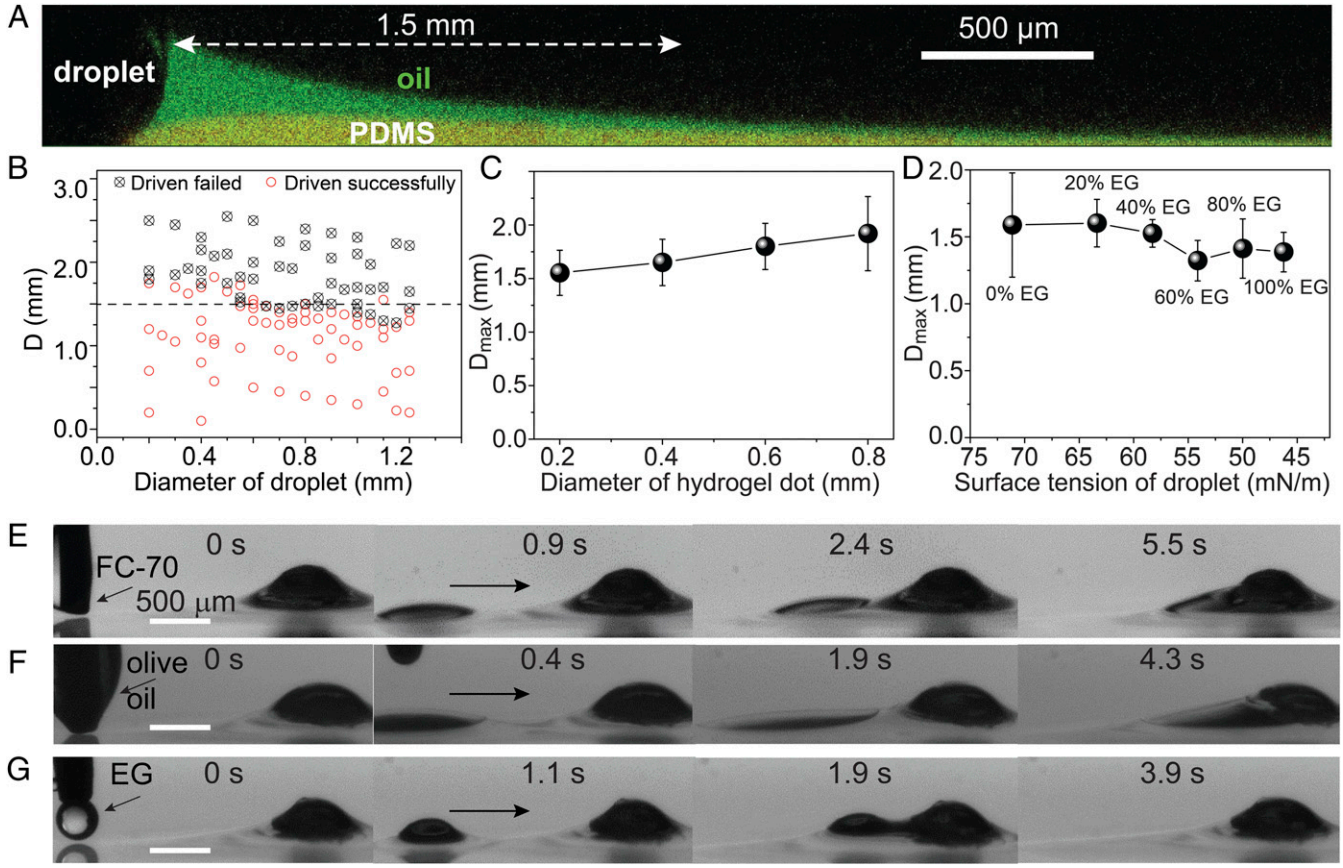

Fig. 2. Water and oil microdroplets can be robustly driven. The driving capability is dependent on the oil meniscus, with the maximum driving distance approximately equal to the meniscus length, i.e., the capillary length (λ). (*A*) Confocal fluorescence image showing the green-dyed oil meniscus, with a length approximately equal to λ = 1.5 mm. (*B*) Results for 100 microdroplets with different diameters and different distances (*D*) to the hydrogel dot, showing that the maximum driving distance (D_{max}) is around 1.5 mm (dashed line). (*C*) D_{max} stays at around 1.5–2.0 mm for various hydrogel dot diameters. (*D*) D_{max} is around 1.5 mm for droplets of different surface tensions from 72 to 47 mN/m, which is obtained by adding different ratios of ethylene glycol (EG) to water. (*E–G*) Low-surface tension oil droplets, including Fluorinert FC-70, olive oil, and EG, with a distance of ∼1.5 mm can also be driven to the hydrogel dot in a few seconds.

syringe. Regardless of the diameter, those droplets deposited beyond D_{max} ∼ 1.5 mm mostly failed to be driven, whereas those deposited closer than D_{max} were successfully driven (Fig. 2*B*). Large droplets with a size of 5 mm were also observed to be successfully driven (*SI Appendix*, Fig. S4). To test the driving of extremely small droplets, we sprayed aerosolized water droplets with a diameter of ∼0.1 mm on the surface and visualized the successful driving (*SI Appendix*, Fig. S5). Our capillary pumping strategy should be applicable to all droplet sizes, but smaller droplets are difficult to generate reliably and thereby not tested. Furthermore, we also investigated the driving capability on hydrogel dots with different sizes and droplets of different surface tensions. Results show that D_{max} stays at around 1.5 mm and is relatively insensitive to the diameter of hydrogel dots (Fig. 2*C*). In addition, D_{max} is also largely independent of hydrogel dot height (*SI Appendix*, Fig. S6). The surface tension of water can be tuned from 72 to 47 mN/m by adding different concentrations of ethylene glycol (EG). Within this range, the maximum driving distance D_{max} was kept at ∼1.5 mm (Fig. 2*D*). This result remains true even for micro-oil droplets despite their low surface tensions. Fig. 2 *E–G* show that pure EG (47 mN/m), olive oil (32 mN/m), and 3M Fluorinert FC-70 (18 mN/m) droplets at ∼1.5 mm away were driven toward the hydrogel dots within a few seconds, even though they have low contact angles. However, it is interesting to note that for lower-surface tension liquid, the driving velocity is generally slower (compare Fig. 3 *E–G* and *SI Appendix*, Fig. S3*A*). This is probably because the contact angle of low-surface tension liquid on lubricant oil is lower, leading to larger contact area and larger viscosity force. Our capillary pumping strategy is therefore universally applicable to all liquid droplets immiscible with the infused oil. Replacing silicone oil infused PDMS with fluorinated oil infused slippery surface (19), which is immiscible with most common liquids, will make this strategy applicable to an even wider range of liquids. Compared with previously reported self-propelled droplet transporting strategies (*SI Appendix*, Fig. S6 and Table S1), only our strategy allows the driving of both water and oil droplets with submillimeter sizes without the need of coalescence. The minimum size of the droplet that can be driven successfully is also among the smallest. Thanks to the low hysteresis nature of our slippery surface, our strategy also resulted in the highest reported driving speed (∼10 mm/s) compared with previous strategies (*SI Appendix*, Fig. S7).

Another remarkable feature of our method is its continuous driving capability. For traditional methods that rely on geometric asymmetry or surface tension gradient, the driving capability is disabled once the asymmetric or gradient region is covered by collected droplets (7). However, for our method, the fluidic oil meniscus is regenerated after each droplet collection, exerting continuous capillary forces to surrounding droplets. Fig. 3*A* shows three water droplets that were driven to the hydrogel dot in sequence. The continuous driving capability of microdroplets due to the hydrogel dots is highly beneficial to water collection. As a proof-of-concept, aerosol water droplets were sprayed onto the surface (Movie S2), and the droplet collection efficiency was

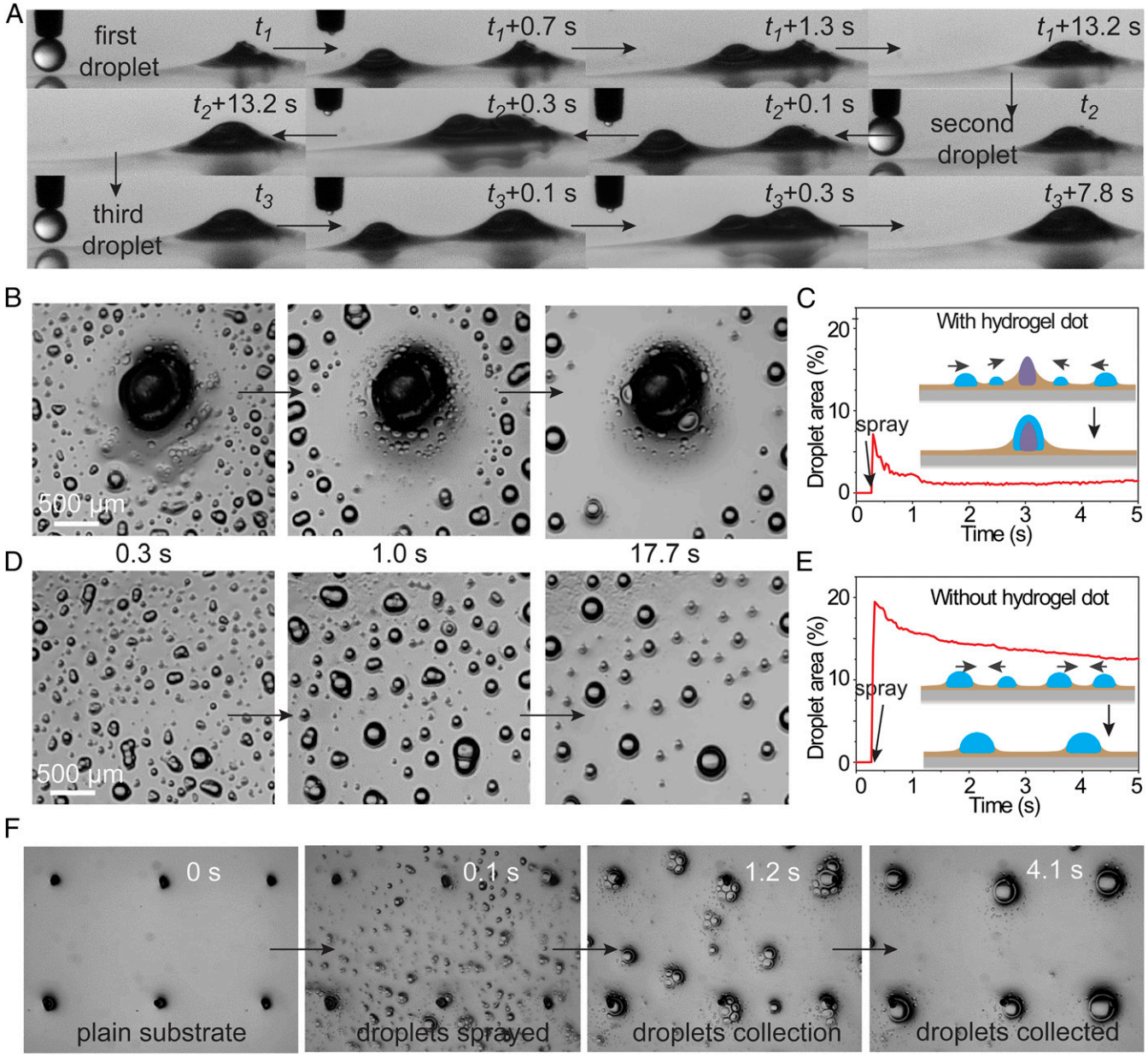

Fig. 3. Continuous capillary pumping for high-efficiency droplet collection. (*A*) Thanks to the self-regeneration of the oil meniscus after each droplet collection, microdroplets can be continuously pumped to the hydrogel dot. The optical images show three water droplets driven to the hydrogel dot in sequence. (*B*) The continuous microdroplet pumping enables high-efficiency water droplet collection. Optical images show that almost all sprayed aerosol microdroplets near the hydrogel dot were rapidly and sequentially pumped to the hydrogel dot. (*C*) As a result, the area fraction covered by the droplet is kept low and gradually decreased to ~2% after spraying. (*D*) On the contrary, without the hydrogel dot, the sprayed aerosol microdroplets randomly coalesced. (*E*) The resultant area fraction covered by the droplet is much higher. (*F*) Hydrogel dots can be patterned into arrays for larger-scale droplet collection.

characterized. For comparison, the same amount of water was sprayed onto another lubricated PDMS surface without the hydrogel dots. With the presence of the hydrogel dots, aerosol droplets were rapidly and continuously driven toward the hydrogel dots (Fig. 3*B* and schematic illustration in Fig. 3*C*, *Inset*). Due to the rapid driving, the fraction of droplet-covered area reached less than 10% immediately after spraying and then quickly decreased to ~2% (Fig. 3*C*). In contrast, the fraction of area covered by droplets PDMS surface without the dots reached 20% immediately after spraying (left image in Fig. 3 *D* and *E*) and decreased gradually to about 15% after a few seconds due to random coalescence of neighboring droplets (middle and right images of Fig. 3*D*, and schematic illustration in Fig. 3*E*, *Inset*). The highly efficient droplet collection should be highly beneficial for droplet condensation and fog harvesting. The hydrogel dots can also be patterned in a large area for larger-scale collection of microdroplets (Fig. 3*F* and Movie S3).

Furthermore, we demonstrate that the high-efficiency aerosol droplet collection can be used in highly sensitive biomedical analysis. Detecting aerosol analytes, such as pathogen-containing respiratory aerosolized droplets (33–35), remains a great challenge due to the small droplet size and low concentration. Our capillary pumping method can significantly enrich analytes onto the hydrogel dots, which substantially increases the detection sensitivity (Fig. 4*A*). As a demonstration, we sprayed aerosol green fluorescent protein (GFP)-tagged *Escherichia coli* (*E. coli*,

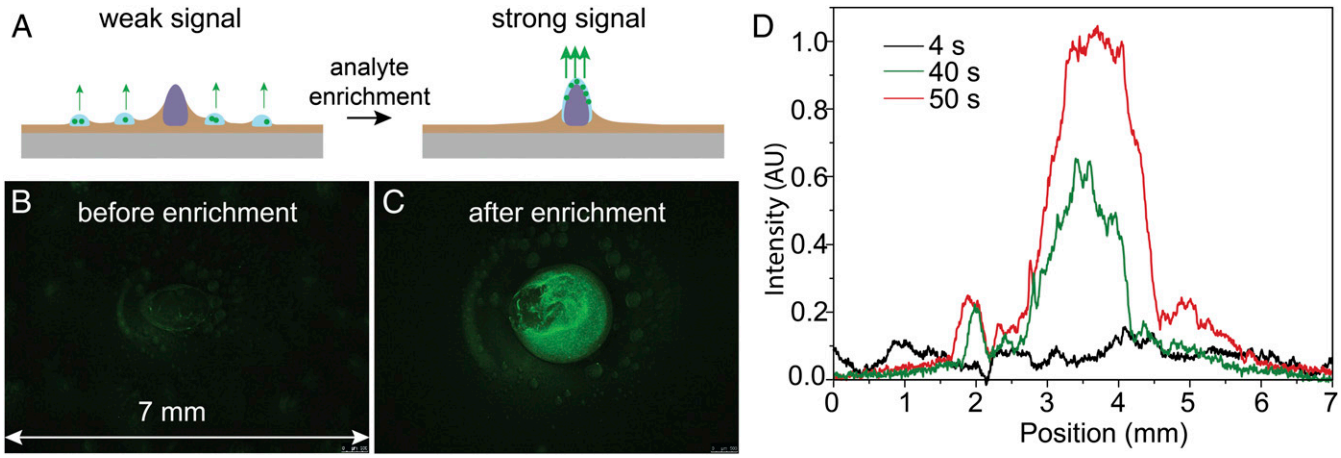

Fig. 4. Highly sensitive detection of aerosol biomedical analyte enabled by the high-efficiency droplet collection. (*A*) Schematic illustration showing the detection method. Aerosol droplets containing biomedical analytes are collected by the hydrogel dots, which substantially enriches the analytes, thereby greatly increasing the sensitivity. (*B*) Sprayed aerosol GFP-expressing *E. coli* (green) showed weak fluorescence intensity. (*C*) After the aerosol droplets were collected by the hydrogel dots (center), *E. coli* was enriched at the center and showed strong fluorescence intensity. (*D*) Average intensity vs. position at different times after spraying.

a bacterium) on our substrate. The hydrogel dot does allow the bacteria to enter due to the lack of large enough pores (*SI Appendix*, Fig. S8). Fluorescence images show that 4 s after spraying, *E. coli* can be hardly detected (Fig. 4*B*). The fluorescent signal (averaged over the vertical positions) is low and widely distributed (Fig. 4*D*). However, after 50 s, microdroplets containing *E. coli* aggregated by the hydrogel dot at the center show strong and centered fluorescent signal (Fig. 4 *C* and *D*). Notably, the fluorescent intensity was increased by nearly an order of magnitude. For practical applications, it could be helpful to use patterned arrays of hydrogel dots to realize multisite enrichment and analysis (*SI Appendix*, Fig. S9). Bacterial killing can also be realized by preimmobilizing biocides on the hydrogel dots (*SI Appendix*, Fig. S10). Note that although natural bacteria are not fluorescent, they can be stained with fluorescent molecules, enabling detection (*SI Appendix*, Fig. S11). Highly sensitive label-free detection could also be realized if combined with other analytical methods such as Raman spectroscopy or mass spectrometry. If the analyte is mixed with gold nanoparticles before or after enrichment, highly sensitive surface-enhanced Raman scattering detection should be possible (36).

In summary, we developed a strategy for directional transport of microdroplets on slippery liquid-infused surfaces. Single microdroplets could be transported and collected by capillary pumping. Such strategy is unprecedentedly easy and highly robust. This strategy can drive both oil and water microdroplets with submillimetric sizes. This strategy could be used in applications including fog harvesting, droplet condensation, and highly sensitive biomedical analysis. We envision that by adopting active surface (37), for example, by incorporating patterned smart hydrogel dots whose shape responses to external stimuli, or even by creating complex surface-piercing structures with ferrofluids in magnetic field, it is possible to fabricate smart droplet fluidic devices.

Methods

Material Fabrication. The 4 wt % sodium alginate (Sigma-Aldrich) solution was printed onto thermally curable PDMS precursor (Dow Corning Sylgard 184, 10:1 base and curing agent). PDMS precursor was spin-coated on a clean glass slide at a rotating speed of 3,000 rpm by using a spin-coater (KW-4A, Institute of Microelectronics of Chinese Academy of Sciences). A dispensing system (AD1520; Biodot) was applied to print alginate sodium solution on liquid PDMS precursor film. The resulting sample was annealed at 80 °C for 5 h before immersed into a 500 mM $CaCl_2$ solution for 0.5 h for the gelation of hydrogel dots. Then the PDMS film was immersed into silicone oil (10cSt; Sigma-Aldrich) for 5 h to swell the PDMS and form an immobilized lubricant meniscus. To control the thickness of the overcoated layer, the oil on the surface was gently wiped by filter papers, and the same oil with controlled volume was added to a known surface area of the sample. GFP-expressing *E. coli* was used in the test of bacterial collection and detection.

Characterization. Microdroplets were generated by two methods: the spraying method and the single-droplet method. For the spraying method, a thin film chromatography sprayer (250 mL; Sigma Aldrich) was used to generate the microdroplets. The sprayer was placed at about 15 cm distance to the surface and sprayed for one time in a single experiment. Alternatively, microdroplets with controlled diameter were generated individually by a homemade superhydrophobic needle. The microdroplet movements were recorded by a horizontally placed microscope equipped with a high-speed CCD (i-speed 3; Olympus). The fluorescent images in the collection and detection of bacteria were acquired by fluorescent microscope (Leica MZ10F Fluorescent Stereomicroscope and Nikon Eclipse Ni-E Fluorescent Microscope).

Further details on the methods are available in the *SI Appendix*.

ACKNOWLEDGMENTS. We thank Prof. J Aizenberg for helpful and detailed discussion on this manuscript. This work was supported by National Natural Science Foundation of China Grant 21501145, General Research Fund (GRF) Hong Kong Grant 21214215, and Collaborative Research Fund (CRF) Hong Kong Grant C1018-17G.

1. Liu M, Wang S, Jiang L (2017) Nature-inspired superwettability systems. *Nat Rev Mater* 2:17036–17052.
2. Lv JA, et al. (2016) Photocontrol of fluid slugs in liquid crystal polymer microactuators. *Nature* 537:179–184.
3. Cira NJ, Benusiglio A, Prakash M (2015) Vapour-mediated sensing and motility in two-component droplets. *Nature* 519:446–450.
4. Daniel S, Chaudhury MK, Chen JC (2001) Fast drop movements resulting from the phase change on a gradient surface. *Science* 291:633–636.
5. Jokinen V, Leinikka M, Franssila S (2009) Microstructured surfaces for directional wetting. *Adv Mater* 21:4835–4838.
6. Chu KH, Xiao R, Wang EN (2010) Uni-directional liquid spreading on asymmetric nanostructured surfaces. *Nat Mater* 9:413–417.
7. Ju J, et al. (2012) A multi-structural and multi-functional integrated fog collection system in cactus. *Nat Commun* 3:1247–1252.
8. Ichimura K, Oh SK, Nakagawa M (2000) Light-driven motion of liquids on a photoresponsive surface. *Science* 288:1624–1626.
9. Chaudhury MK, Whitesides GM (1992) How to make water run uphill. *Science* 256:1539–1541.
10. Chen H, et al. (2016) Continuous directional water transport on the peristome surface of Nepenthes alata. *Nature* 532:85–89.

11. Malvadkar NA, Hancock MJ, Sekeroglu K, Dressick WJ, Demirel MC (2010) An engineered anisotropic nanofilm with unidirectional wetting properties. *Nat Mater* 9:1023–1028.
12. Li J, et al. (2016) Oil droplet self-transportation on oleophobic surfaces. *Sci Adv* 2:e1600148.
13. Prakash M, Quéré D, Bush JWM (2008) Surface tension transport of prey by feeding shorebirds: The capillary ratchet. *Science* 320:931–934.
14. Wang Q, Yao X, Liu H, Quéré D, Jiang L (2015) Self-removal of condensed water on the legs of water striders. *Proc Natl Acad Sci USA* 112:9247–9252.
15. Cho HJ, Preston DJ, Zhu YY, Wang EN (2017) Nanoengineered materials for liquid-vapour phase-change heat transfer. *Nat Rev Mater* 2:16092–16108.
16. Zheng Y, et al. (2010) Directional water collection on wetted spider silk. *Nature* 463: 640–643.
17. Liu J, et al. (2016) Guided self-propelled leaping of droplets on a micro-anisotropic superhydrophobic surface. *Angew Chem Int Ed Engl* 55:4265–4269.
18. Boreyko JB, Chen CH (2009) Self-propelled dropwise condensate on superhydrophobic surfaces. *Phys Rev Lett* 103:184501.
19. Wong TS, et al. (2011) Bioinspired self-repairing slippery surfaces with pressure-stable omniphobicity. *Nature* 477:443–447.
20. Park KC, et al. (2016) Condensation on slippery asymmetric bumps. *Nature* 531:78–82.
21. Peruzzo P, Defina A, Nepf HM, Stocker R (2013) Capillary interception of floating particles by surface-piercing vegetation. *Phys Rev Lett* 111:164501.
22. Peruzzo P, Defina A, Nepf H (2012) Capillary trapping of buoyant particles within regions of emergent vegetation. *Water Resour Res* 48:W07512.
23. Hu DL, Bush JWM (2005) Meniscus-climbing insects. *Nature* 437:733–736.
24. Pokroy B, Kang SH, Mahadevan L, Aizenberg J (2009) Self-organization of a mesoscale bristle into ordered, hierarchical helical assemblies. *Science* 323:237–240.
25. Jiang J, et al. (2016) Fabrication of transparent multilayer circuits by inkjet printing. *Adv Mater* 28:1420–1426.
26. Cavallaro M, Jr, Botto L, Lewandowski EP, Wang M, Stebe KJ (2011) Curvature-driven capillary migration and assembly of rod-like particles. *Proc Natl Acad Sci USA* 108: 20923–20928.
27. Paunov VN, Kralchevsky PA, Denkov ND, Nagayama K (1993) Lateral capillary forces between floating submillimeter particles. *J Colloid Interface Sci* 157:100–112.
28. Danov KD, Pouligny B, Kralchevsky PA (2001) Capillary forces between colloidal particles confined in a liquid film: The finite-meniscus problem. *Langmuir* 17:6599–6609.
29. Batchelor GK (2000) *An Introduction to Fluid Dynamics* (Cambridge Univ Press, Cambridge, United Kingdom).
30. Daniel D, Timonen JVI, Li RP, Velling SJ, Aizenberg J (2017) Oleoplaning droplets on lubricated surfaces. *Nat Phys* 13:1020–1025.
31. Keiser A, Keiser L, Clanet C, Quéré D (2017) Drop friction on liquid-infused materials. *Soft Matter* 13:6981–6987.
32. Schellenberger F, et al. (2015) Direct observation of drops on slippery lubricant-infused surfaces. *Soft Matter* 11:7617–7626.
33. Sorrell EM, Wan H, Araya Y, Song H, Perez DR (2009) Minimal molecular constraints for respiratory droplet transmission of an avian-human H9N2 influenza A virus. *Proc Natl Acad Sci USA* 106:7565–7570.
34. Zhang Q, et al. (2013) H7N9 influenza viruses are transmissible in ferrets by respiratory droplet. *Science* 341:410–414.
35. Imai M, et al. (2012) Experimental adaptation of an influenza H5 HA confers respiratory droplet transmission to a reassortant H5 HA/H1N1 virus in ferrets. *Nature* 486:420–428.
36. Yang S, Dai X, Stogin BB, Wong T-S (2016) Ultrasensitive surface-enhanced Raman scattering detection in common fluids. *Proc Natl Acad Sci USA* 113:268–273.
37. Wang W, et al. (2018) Multifunctional ferrofluid-infused surfaces with reconfigurable multiscale topography. *Nature* 559:77–82.